# Independent regulation of the lithium-ion conductivity of LiF using elemental doping: A first-principles study

Na Yang ©, Xian-Qi Xu ©,* and Jia-Xin Zheng ©†

*School of Advanced Materials, Peking University, Shenzhen Graduate School, Shenzhen 518000, People's Republic of China*

Lithium fluoride (LiF) is an important component of solid electrolyte interphase (SEI), but its low ionic conductivity limits the applications in lithium-ion batteries. In order to obtain high-performance SEI layers, we wanted to improve lithium-ion conductivity of LiF by doping at low concentrations while minimizing damage to electronic conductivity and maintaining high mechanical strength. First-principles calculations were performed to initially screen the main group elements, of which Na, K, Be, Mg, Ca, and Al were found to meet this material design requirement. Further, the effect of these elemental dopings on the properties of the bulk, surface, and interfacial phases was systematically investigated. We demonstrate that monovalent ion doping increases lithium-ion conductivity mainly by lowering the diffusion energy barrier, whereas multivalent ion doping increases lithium-ion conductivity by inducing lithium negatively charged vacancy. Divalent ions ($Be^{2+}$, $Mg^{2+}$, and $Ca^{2+}$) are recommended for doping into lithium fluoride because they increase the lithium-ion conductivity by 18 orders of magnitude with insignificant decreases in electronic conductivity and mechanical strength. Our work provides theoretical guidance and a research paradigm for the preparation of artificial SEI films with excellent properties.

DOI: 10.1103/PhysRevMaterials.8.015403

## I. INTRODUCTION

Solid electrolyte interphase (SEI) is a thin passivation film produced at the solid-liquid interface by reaction between the anode and the electrolyte, and has been shown to be effective in increasing the cycle life of lithium-ion batteries (LIBs). This film has highly mechanical and electronic insulating properties acting as a natural electron/space barrier to prevent further electrolyte consumption and lithium dendrite growth, while allowing free insertion and extraction of Li ions during battery operation [1]. However, it is difficult to find a SEI material that simultaneously satisfies high mechanical property, high electronic insulation, and high ionic conductivity. Therefore, there is a strong necessity to investigate techniques to independently modulate the properties of the material, i.e., to modulate one property while keeping the other properties unchanged.

To better understand the composition and structure of SEI, the researchers have used experimental techniques such as x-ray photoelectron spectroscopy (XPS), cryoelectron microscopy (cryo-EM), cryoscanning transmission electron microscopy (cryo-STEM), and electron energy loss spectroscopy (EELS) to characterize it [1]. The experimental results show that typical SEI compositions mainly include LiF, $Li_2O$, $Li_2CO_3$, $Li_3N$, and LiOH [2]. Among these components, LiF has gained the most attention due to its excellent electronic insulation and superior mechanical strength. There are two options for obtaining LiF-containing SEI: (i) Adding fluorine-containing lithium salts, organic solvents,

or additives to change the composition of the electrolyte. Wang's group [3] increased the concentration of LiFSI in the electrolyte to facilitate the formation of LiF-rich SEI. Zhang's group [4] added both fluoroethylene carbonate (FEC) and $LiNO_3$ to the electrolyte to produce $LiN_xO_y$-LiF-rich SEI, which resulted in uniform lithium deposition and exceptional cycling stability of up to 1000 cycles. (ii) Creating an artificial SEI by depositing LiF on the electrode surface using growth techniques such as atomic layer deposition (ALD) or magnetron sputtering. Cui's group [5] employed the ALD technique to grow LiF on hexagonal boron nitride (h-BN) to form a hybrid LiF/h-BN film. The films are effective in inhibiting lithium dendrite formation and provide excellent cycling stability for LIBs. Lang *et al.* [6] reported a facile and cost-effective solution-based chemical reaction method for preparing LiF film on lithium metal anode. Batteries assembled with this anode exhibited excellent cycling stability of over 300 cycles at a high current density of $3 \, mA \, cm^{-2}$.

However, Li-ion conductivity for LiF is unsatisfactory because it is reported to be below $10^{-12}$ S/m [7–10]. To address this problem, Hu *et al.* [11] have successfully synthesized a $Li_3Sb$/LiF artificial hybrid interphase through a facile solution reaction to effectively enhanced the Li diffusion across the entire interface. Ren *et al.* [12] attempted to accelerate Li diffusion kinetics of LiF by heavy doping with La elements. Pan's group [13] suggested doping LiF with divalent cations to improve the conductivity of lithium ions, but the effectiveness and mechanism of this suggestion has not been proven. To our knowledge, only a very small number of LiF modification studies have considered simultaneously electronic conductivity, Li-ion conductivity, and mechanical strength.

In this paper, we used first-principles calculations to screen suitable candidates from main group elements and eventually

---

*Corresponding author: xuxianqi@pku.edu.cn
†Corresponding author: zhengjx@pkusz.edu.cn

targeted the elements $Na^+$, $K^+$, $Be^{2+}$, $Mg^{2+}$, $Ca^{2+}$, and $Al^{3+}$ for doping into LiF. Then density functional theory (DFT) calculations were performed to investigate the effects of doping with target elements on the performance of LiF-SEI including: Li-ion conductivity, electronic conductivity, and mechanical strength. The diffusion energy barrier was calculated by the climbing image-nudged elastic band (CI-NEB) method and the ionic conductivity was obtained based on the Nernst-Einstein equation. The electronic conductivity was estimated by combining the deformation potential theory and the Boltzmann distribution approximation function. The goal of this work is to increase the Li-ion conductivity without compromising the electronic insulation and mechanical strength.

## II. METHOD

### A. Details of the DFT calculations

Density functional theory (DFT) calculations were employed with the projector augmented wave (PAW) method in the Vienna *Ab initio* Simulation Package (VASP) [14]. The generalized gradient approximation (GGA) with the parametrization of Perdew-Burke-Ernzerhof (PBE) was used to explain exchange-correlation functional [15,16]. A plane-wave cutoff energy of 520 eV was applied for all the calculations. The convergence of energy and forces were set at $10^{-5}$ eV/atom and 0.02 eV/Å, respectively. The crystal LiF has a rock salt structure with the space group of $Fm\bar{3}m$ [17,18]. Three models are considered: (i) bulk LiF; (ii) the (001) surface of LiF, which has the lowest surface energy [19]; (iii) LiF(001)-Li(001) interface. Cell parameters and k points are listed in Supplemental Material, Tables S1–S3 [20]. For the surface and interface models, we set a vacuum layer of 15 Å. In the charged defects calculation, we add (subtract) an electron to (from) the total valence electrons in LiF. For example, we add one electron to the supercell with Li negatively charged vacancy, i.e., $V_{Li}^-$. The climbing image-nudged elastic band (CI-NEB) method [21,22] was implemented to obtain the migration energy barrier of points defects. Five images were inserted between initial and final states. All images are optimized simultaneously until the forces acting on the atoms converge to 0.05 eV/Å. The band gap calculations are also performed with Heyd-Scuseria-Ernzerhof (HSE06) hybrid exchange correction functional [23] using PWMAT [24]. Bader charge analysis was simply implemented using Henkelman group's code [25,26]. In this method, the continuous distribution of electron densities is partitioned to each atom based on the lowest value of the atomic charge density. And we performed DFT calculations to determine the number of valence electrons for each atom.

### B. Formation energy

The formation energy for a defect $[X]$ in a specific charge state $q$ is calculated as follows [27,28]:

$$\Delta E_{X,q} = E_{X,q} - E_b - \sum_i n_i \mu_i + q(E_{vbm} + E_{Fermi}) + E_{corr},$$

$$(1)$$

where $E_{X,q}$ and $E_b$ are the total energy of the supercell with and without defects, $n_i$ and $\mu_i$ represent the number

and chemical potential of the removed (added) atom. $\mu_{Li}$ is a variable parameter depending on the nature of the coating electrode [29]. There are two circumstances: (i) $\mu_{Li}$ reaches the upper bound when LiF is attached to the Li metal: $\mu_{Li}^{max} = \mu_{Li}^{metal} = -1.9\,eV$; (ii) $\mu_{Li}$ reaches the lower bound when LiF is attached to the positive electrode [30]: $\mu_{Li}^{min} = \mu_{Li}^{metal} - 4.6\,eV = -6.5\,eV$. Only Li-rich condition is considered in this research. The $\mu_F$ value is constrained by Eq. (2),

$$\mu_F = \mu_{LiF} - \mu_{Li}. \qquad (2)$$

$E_{vbm}$ is the energy of valence band maximum, $E_{Fermi}$ is the Fermi energy, also known as the electron chemical potential, which is referenced to the valence band maximum; $E_{corr}$ is the correction terms included [29,31,32]: (i) Potential correction: aligning the valence band maximums between defective and perfect crystals, the average static potential difference between cells with and without charged defects. (ii) Dispersion correction: remediate elastic interactions between charged defect and its periodic images. (iii) Makov-Payne correction: $\alpha q^2(1/\varepsilon L)$ in which $\alpha$, $\varepsilon$, and $L$ are Madelung constant, dielectric constant, and supercell dimension. All the correction terms are related to finite-sized cells and periodic boundary conditions. Therefore, $E_{corr}$ is not considered if the supercell is large enough. Qi's research [13] suggests $E_{corr}$ (only 0.03 eV) is too small to change the defect concentration in magnitude. So the correction term is neglected.

### C. Concentration of electron and defect

It is worth noting that the $E_{Fermi}$ in Eq. (1) is not the Fermi energy of the DFT calculation, but determined by the condition of electroneutrality [27,33,34]:

$$\sum_{X,q} q n(X, q) + n_h - n_e = 0. \qquad (3)$$

$n(X, q)$ is the concentration of the defect $X$. $n_e$ and $n_h$ represent electron and hole concentrations. At finite temperature $T$, the concentration of defect $X$ is defined as [27,35]:

$$n(X, q) = N_s(X) \exp\left(-\frac{\Delta E_{X,q}}{k_B T}\right), \qquad (4)$$

where $N_s(X)$ denotes the number of the lattice sites per unit volume that can generate defect $X$, $k_B$ is Boltzmann constant, and $T$ is set to 300 K. In Li-rich condition, $V_{Li}^-$ and $V_F^+$ are present simultaneously with the same formation energy. The main defect of LiF becomes the dilute pair consisting of $V_{Li}^-$ and $V_F^+$, so Eq. (4) can be converted to

$$n(X, q) = N_s(X) \exp\left(-\frac{\Delta E_{act}}{k_B T}\right), \qquad (5)$$

where $\Delta E_{act} = \Delta E_{V_{Li}^-} + \Delta E_{V_F^+}$ [13].

In thermal equilibrium, the electron concentration of nondegenerate semiconductors is [36]

$$n_e = \int_{E_{cbm}}^{E'_{cbm}} 4\pi \frac{(2m_e^*)^{3/2}}{h^3}$$

$$\times \exp\left(-\frac{E - E_{Fermi}}{k_B T}\right)(E - E_{cbm})^{1/2} dE, \qquad (6)$$

the upper limit of integration $E'_{cbm}$ is the energy of the conduction band maximum. For LiF, the carrier concentration is low and the Boltzmann approximation can be applied to simplify Eq. (6),

$$n_e \approx \frac{(m_e^* k_B T)^{3/2}}{2\pi \hbar^2} \exp\left(-\frac{E_{cbm} - E_{Fermi}}{k_B T}\right) \qquad (7)$$

$$n_h \approx \frac{(m_h^* k_B T)^{3/2}}{2\pi \hbar^2} \exp\left(\frac{E_{vbm} - E_{Fermi}}{k_B T}\right), \qquad (8)$$

where $m_e^*$ and $m_h^*$ are electron and hole effective mass, which are obtained by making a second-order derivative from the band at valence band maxima and conduction band minima $[\partial^2 E(k)/\partial k^2]$. $\hbar$ is reduced Planck constant: $\hbar = h/(2\pi)$ and $E_{cbm}$ is the energy of conduction band minimum. Simultaneous Eqs. (3), (4), (7), and (8), equilibrium Fermi energy ($E_{Fermi,eq}$), the defect concentration, and electron concentration can be derived self-consistently.

### D. Defect diffusion coefficient and carrier mobility

The diffusion coefficient $D$ with finite temperature $T$ and migration energy barrier $E_m(X, q)$ is [37]

$$D = g(\Delta x)^2 \nu \exp\left(-\frac{E_m(X, q)}{k_B T}\right), \qquad (9)$$

where $g$ is the dimensionality of diffusion (1-3), $\nu$ is the phonon frequency ($\nu \approx 10^{13} s^{-1}$) and $\Delta x$ is the diffusion distance.

The carrier mobility $\zeta_{ij}$ is obtained from the theory of deformation potential [38,39]:

$$\zeta_{ij} = \frac{(8\pi)^{1/2} \hbar^4 e C_{ij}}{3(m_{ij}^*)^{5/2}(k_B T)^{3/2} D_{ij}^2}, \qquad (10)$$

where $m_{ij}^*$ is the effective mass tensor and $C_{ij}$ is the elastic constant. The deformation potential $D_{ij}$ is obtained by $D_{ij} = \Delta E_{vbm(cbm)}/(\Delta l/l_0)$, which depicts the deformation potential constant for holes/electrons at vbm/cbm along the transport orientation. $\Delta E$ is the variation in energy of the vbm/cbm under compressive and tensile strain. $l_0$ and $\Delta l$ are the lattice constant and deformation in the transport direction, respectively.

### E. Lithium-ion conductivity and electron conductivity

The Nernst-Einstein equation [40,41] develops an association between the ionic conductivity $\sigma$ and the diffusion coefficient $D$:

$$\sigma = D\frac{nq^2}{k_B T}, \qquad (11)$$

where $n$ is the defect concentration per unit volume. The lithium-ion conductivity in LiF attracts much attention, which relies mainly on $V_{Li}^-$, so Eq. (11) can be converted to

$$\sigma = \sigma_{V_{Li}^-} = D_{V_{Li}^-}\frac{nq^2}{k_B T}. \qquad (12)$$

Calculation formula for electron conductivity is [42,43]

$$\sigma_e = n_e e \zeta, \qquad (13)$$

where $e$ is the electron charge.

## III. RESULTS AND DISCUSSION

### A. LiF bulk

#### 1. Defects concentration

Low Li-ion conductivity is an undesired property that limits the application of LiF in LIBs. Considering the fitness of atomic radii and the fact that transition elements can introduce d-band electrons to weaken electronic insulation [44,45], here we attempted to improve Li-ion conductivity by doping with the main group elements of period 2 to period 4 (Be, B, C, N, O, Na, Mg, Al, Si, P, S, Cl, K, Ca, Ga, Ge, As, Se, and Br) while keeping the other properties constant. The elements in group IV A to group VII A prefer F-site doping, C, N, O, Si, P, S, Ge, As, and Se doping will introduce excess $V_F^+$, which is useless for Li diffusion because Li migration to the $V_F^+$ position is unstable. However, the diffusion energy barrier is very high after doping with Cl and Br, neither of which is conducive to achieving our goal. So C, N, O, Si, P, S, Cl, Ge, As, Se, and Br doping is not considered. In addition, the elements B and Ga have been excluded because they have high doping formation energy. Ultimately, Na, K, Be, Mg, Ca, and Al were chosen for further studies, and doping formation energy calculations demonstrate that these ions can be doped into LiF. The results and discussion of these calculations can be found in Supplemental Material, Table S4 [20].

Defect formation energy is a key factor in determining the concentration of defects. The lower the defect formation energy, the easier it is to form defects and the higher the concentration will be. The LiF structure models for defect formation energy calculations are shown in Fig. 1, where an impurity ion replaces a Li ion. Since the diffusion of paired defects does not contribute significantly to the ionic conductivity [13,46], we considered all possible individual defects (Li negatively charged vacancy: $V_{Li}^-$; Li positively charged interstitial: $Li_i^+$; F positively charged vacancy: $V_F^+$; F negatively charged interstitial: $F_i^-$) and calculated their formation energies by Eq. (1). Figure 2 shows the variation of defect formation energy with Fermi energy. As the system remains electrically neutral, the concentrations of the main defects $V_{Li}^-$ and $V_F^+$ must be equal. According to Eq. (4), the formation energies of these two defects must also be equal. In this case, the concentration of $V_{Li}^-$ is calculated by Eq. (5). The goal of this work is to increase the Li-ion conductivity, so we will only discuss $V_{Li}^-$ in the next representation. Defects $F_i^-$ and $Li_i^+$ are difficult to form because LiF is very compact and their presence disturbs the lattice, causing internal strain and increasing the energy of the system [2]. In pure LiF, $E_{Fermi,eq}$ is at 5.83 eV [Fig. 2(a)], where the formation energy and the concentration of $V_{Li}^-$ are 0.61 eV and $1.87 \times 10^2$ cm$^{-3}$, respectively. When the monovalent ions Na$^+$ and K$^+$ were doped, $E_{Fermi,eq}$ reduce to 5.73 and 5.46 eV, respectively. The formation energy and the concentration of $V_{Li}^-$ are 0.59 eV and $3.41 \times 10^2$ cm$^{-3}$ for Na$^+$ as well as 0.55 eV and $10^{-2}$ cm$^{-3}$ for K$^+$. It is worth noting that the defect formation energy is always negative when doped with multivalent ions (see Fig. S5 [20]), which indicates that the bulk material is thermally unstable and tends to form Li vacancies. These Li vacancies are defined as charge-induced intrinsic defects in this paper [47]. Therefore, we artificially remove Li ions to keep the system charge balanced, e.g., one Li ion is removed
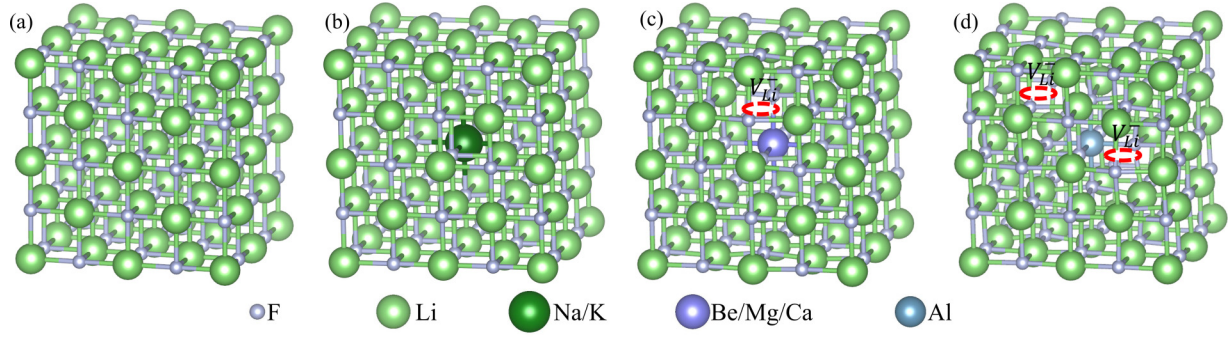
FIG. 1. Schematic diagram of the LiF bulk calculation models. (a) Pure LiF. (b) Monovalent ion-doped LiF. (c) Divalent ion-doped LiF. One $V_{Li}^-$ already exists in the structure. (d) Trivalent ion-doped LiF. Two $V_{Li}^-$ already exist in the structure. All models are Li-site doped and have a doping concentration of 1/64.

for $Be^{2+}$, $Mg^{2+}$, and $Ca^{2+}$ doping [Fig. 1(c)] and two Li ions for $Al^{3+}$ doping [Fig. 1(d)]. To better distinguish the two doping models for LiF, we take Be doped as an example to make the following definition: (i) LiF-Be structure: the host material replaces one Li atom with Be and no vacancy exists. The calculation of defects is based on the LiF-Be structure. The discussions about LiF-Be structure are shown in Supplemental Material, 2.2 [20]. (ii) LiF-Be-$V_{Li}$ structure: the host material replaces one Li with Be and a Li vacancy already exists in the structure. The calculation of defects is based on the LiF-Be-$V_{Li}$ structure. For example, the formation of $V_{Li}^-$ here means having one extra Li vacancy based on the original LiF-Be-$V_{Li}$. All of the following discussions are based on LiF-Be-$V_{Li}$ structure. The location arrangements of dopants and vacancies in the diagram achieve the lowest energy, see Supplemental Material, 2.4 [20]. On the basis of the charge balance, we calculated the formation energy of defects in the multivalent ion doping system. The formation energy of $V_{Li}^-$ is 0.21eV at $E_{Fermi,eq} = 5.65$ eV for LiF-Be-$V_{Li}$ [Fig. 2(d)],

0.74eV at $E_{Fermi,eq} = 5.45$ eV for LiF-Mg-$V_{Li}$ [Fig. 2(e)], and 0.45eV at $E_{Fermi,eq} = 5.54$ eV for LiF-Ca-$V_{Li}$ [Fig. 2(f)]. However, the concentration of defects calculated by Eq. (5) (see Table S5 [20]) is much smaller in order of magnitude than the concentration of charge-induced intrinsic defects. Therefore, for multivalent systems, we only consider the concentration of charge-induced intrinsic defects. The concentrations of $V_{Li}^-$ are $1.88 \times 10^{21}$ cm$^{-3}$, $1.80 \times 10^{21}$ cm$^{-3}$, and $1.75 \times 10^{21}$ cm$^{-3}$ for $Be^{2+}$, $Mg^{2+}$, and $Ca^{2+}$, respectively. Similarly, two $V_{Li}^-$ already exist after doping with $Al^{3+}$. In Fig. 2(g), the formation energy of $V_{Li}^-$ is 0.36 eV at $E_{Fermi,eq} = 5.37$ eV. However, the actual concentration of $V_{Li}^-$ are $3.56 \times 10^{21}$ cm$^{-3}$. The interstitial defects are no longer stable due to the presence of two vacancies, so only $V_{Li}^-$ and $V_F^+$ are shown.

In this section, monovalent ions $Na^+$ and $K^+$ doping have little effect on the $V_{Li}^-$ concentration, while multivalent ions $Be^{2+}$, $Mg^{2+}$, $Ca^{2+}$, and $Al^{3+}$ doping result in charge-induced intrinsic $V_{Li}^-$ to maintain the charge balance, which leads to a sharp increase in $V_{Li}^-$ concentration.
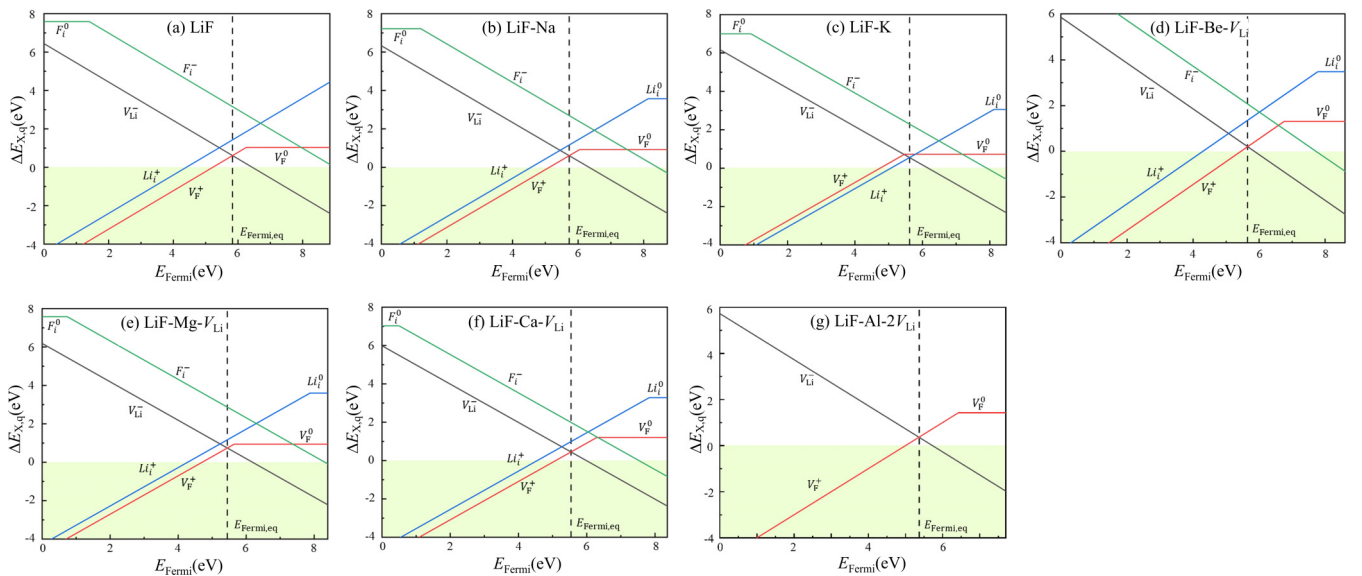


FIG. 2. Formation energy ($\Delta E_{X,q}$) of point defects as a function of Fermi energy ($E_{Fermi,eq}$) under the Li-rich condition ($\mu_{Li} = -1.9$ eV) in (a) LiF, (b) LiF-Na, (c) LiF-K, (d) LiF-Be-$V_{Li}$, (e) LiF-Mg-$V_{Li}$, (f) LiF-Ca-$V_{Li}$, and (g) LiF-Al-2$V_{Li}$. The slope of the curve indicates the defect charge state, the black dashed line depicts the equilibrium Fermi energy, and the light green shaded area shows the case where the defect formation energy is negative. The range of the horizontal coordinates is the band gap.
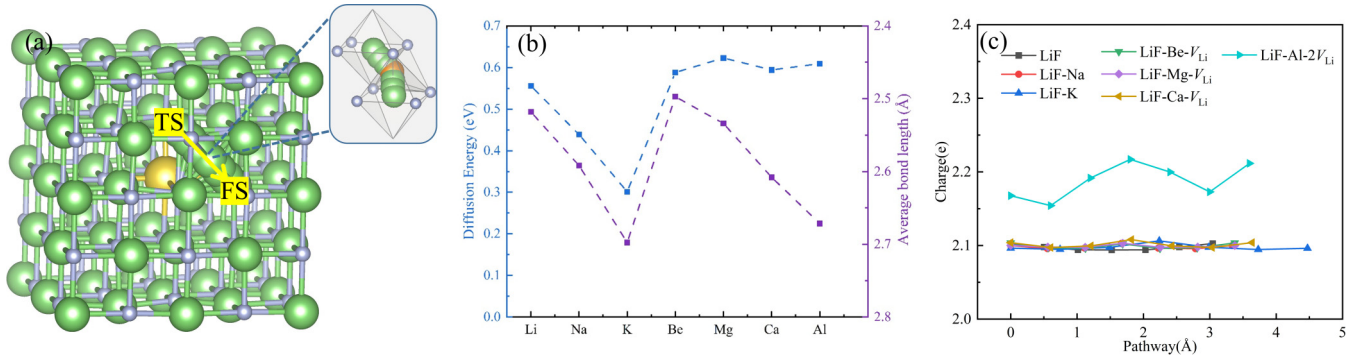
FIG. 3. (a) Schematic diagram of the $V_{Li}^-$ diffusion path in the LiF bulk. TS is initial state and FS is final state. Yellow sphere represents $Na^+$, $K^+$, $Be^{2+}$, $Mg^{2+}$, $Ca^{2+}$, and $Al^{3+}$. Orange sphere represents the $Li^+$ at the saddle point. (b) The diffusion energy barrier and the average bond lengths of migrating ions at the saddle point. (c) The Bader charge value of $Li^+$ for each intermediate state during the diffusion of $V_{Li}^-$.

### 2. Diffusion energy barrier

The diffusivity of defects is another factor affecting Li-ion transport, which can be described by the diffusion energy barrier ($E_a$). The higher the energy barrier, the more difficult the diffusion. To highlight the role of the dopant atoms, we designed Li-ion diffusion paths near the dopant atoms in Fig. 3(a). As shown in Fig. 3(b), the $V_{Li}^-$ diffusion energy barrier in pure LiF is 0.56 eV, which drops to 0.44 and 0.30 eV when doping with the monovalent ions $Na^+$ and $K^+$. This is because $Na^+$ and $K^+$ have larger ionic radii than $Li^+$ and undergo a certain degree of volume expansion during atomic relaxation (see Supplemental Material, Fig. S6 [20]), resulting in larger lattice sizes and smaller steric hindrance. To explain this spatial effect, the average bond length between the migrating ions and the eight nearest neighbors F ions at the saddle point was calculated. The average bond length in pure LiF is 2.52 Å, while this length increases to 2.59 Å and 2.70 Å after doping with $Na^+$ and $K^+$, which demonstrates the reduction in steric hindrance. When doping with $Mg^{2+}$ and $Ca^{2+}$, the average bond length increases to 2.53 Å and 2.61 Å, respectively, indicating a slight reduction in steric hindrance. As for $Be^{2+}$ doping, the average bond length almost unchanged (2.50 Å). It is noteworthy that we calculated the diffusion energy barrier of the charge-induced intrinsic Li vacancy at multivalent ions doping. However, when doped with divalent ions, LiF tends to form a high concentration of $V_{Li}^-$ and this $V_{Li}^-$ is tightly bound to the impurities ($Be^{2+}$, $Mg^{2+}$, and $Ca^{2+}$). At this time, electrostatic interactions are greater than the spatial effects, resulting in more difficult $V_{Li}^-$ diffusion. Therefore, the diffusion energy barriers of $V_{Li}^-$ rise to 0.59, 0.62, and 0.59 eV for $Be^{2+}$, $Mg^{2+}$, and $Ca^{2+}$, respectively. Similarly, compare to pure LiF,

the average bond length and the energy barrier increase to 2.67 Å and 0.61 eV after $Al^{3+}$ doping. Also, we found that the charge was almost constant during Li-ion diffusion, except for a small charge fluctuation in the Al-doped system, so we assume that no charge transfer occurred during this diffusion, see Fig. 3(c). Our analysis shows that the migration energy barrier of Li ions is mainly influenced by steric hindrance and electrostatic interactions.

### 3. Li-ion conductivity

According to the Nernst-Einstein equation [Eq. (11)], Li-ion conductivity depends mainly on the concentration and diffusion coefficient of $V_{Li}^-$. The concentration of $V_{Li}^-$ has been given in Sec. III A 1 and the diffusion coefficient of $V_{Li}^-$ can be calculated using the diffusion energy barriers and the net travel distance of $V_{Li}^-$ based on the Arrhenius formula, which can be found in Eq. (9). For pure LiF, the Li diffusion coefficient $D_{V_{Li}^-}$ is $1.77 \times 10^{-12}$ cm²/s, which is in agreement with Ajaykrishna's work [14]. For the modified LiF, it is found that monovalent ion doping increased the $D_{V_{Li}^-}$ by 2–4 orders of magnitude, whereas multivalent ion doping decreased the $D_{V_{Li}^-}$ by one order of magnitude. Table I lists the values of the Li-ion conductivity and all the key parameters associated with it. According to our calculations, the LiF has a very low Li-ion conductivity of only $2.00 \times 10^{-27}$ S/cm, which is qualitatively consistent with the actual situation. However, after the modification, the Li-ion conductivity was significantly improved. When doping with monovalent ions, the Li-ion conductivity is increased by 1–2 orders of magnitude, mainly due to the increase in diffusion coefficient of $V_{Li}^-$. But when doping with multivalent ions, there is an 18 order of

TABLE I. Parameters of Li-ion conductivity for pure LiF and modified LiF.

| | $E_a$ (eV) | Distance (cm) | $D_{V_{Li}^-}$ (cm²/s) | $n_{V_{Li}^-}$ (cm⁻³) | $\sigma_{V_{Li}^-}$ (S/cm) |
|---|---|---|---|---|---|
| LiF | 0.56 | $2.78 \times 10^{-8}$ | $1.77 \times 10^{-12}$ | $1.87 \times 10^2$ | $2.00 \times 10^{-27}$ |
| LiF-Na | 0.44 | $2.89 \times 10^{-8}$ | $1.77 \times 10^{-10}$ | $3.41 \times 10^2$ | $3.74 \times 10^{-25}$ |
| LiF-K | 0.30 | $3.22 \times 10^{-8}$ | $4.46 \times 10^{-8}$ | $7.02 \times 10^{-2}$ | $1.94 \times 10^{-26}$ |
| LiF-Be-$V_{Li}$ | 0.59 | $2.83 \times 10^{-8}$ | $4.91 \times 10^{-13}$ | $1.88 \times 10^{21}$ | $5.72 \times 10^{-9}$ |
| LiF-Mg-$V_{Li}$ | 0.62 | $2.92 \times 10^{-8}$ | $1.46 \times 10^{-13}$ | $1.80 \times 10^{21}$ | $1.63 \times 10^{-9}$ |
| LiF-Ca-$V_{Li}$ | 0.59 | $3.12 \times 10^{-8}$ | $5.09 \times 10^{-13}$ | $1.75 \times 10^{21}$ | $5.52 \times 10^{-9}$ |
| LiF-Al-$2V_{Li}$ | 0.61 | $3.05 \times 10^{-8}$ | $2.70 \times 10^{-13}$ | $3.56 \times 10^{21}$ | $5.94 \times 10^{-9}$ |
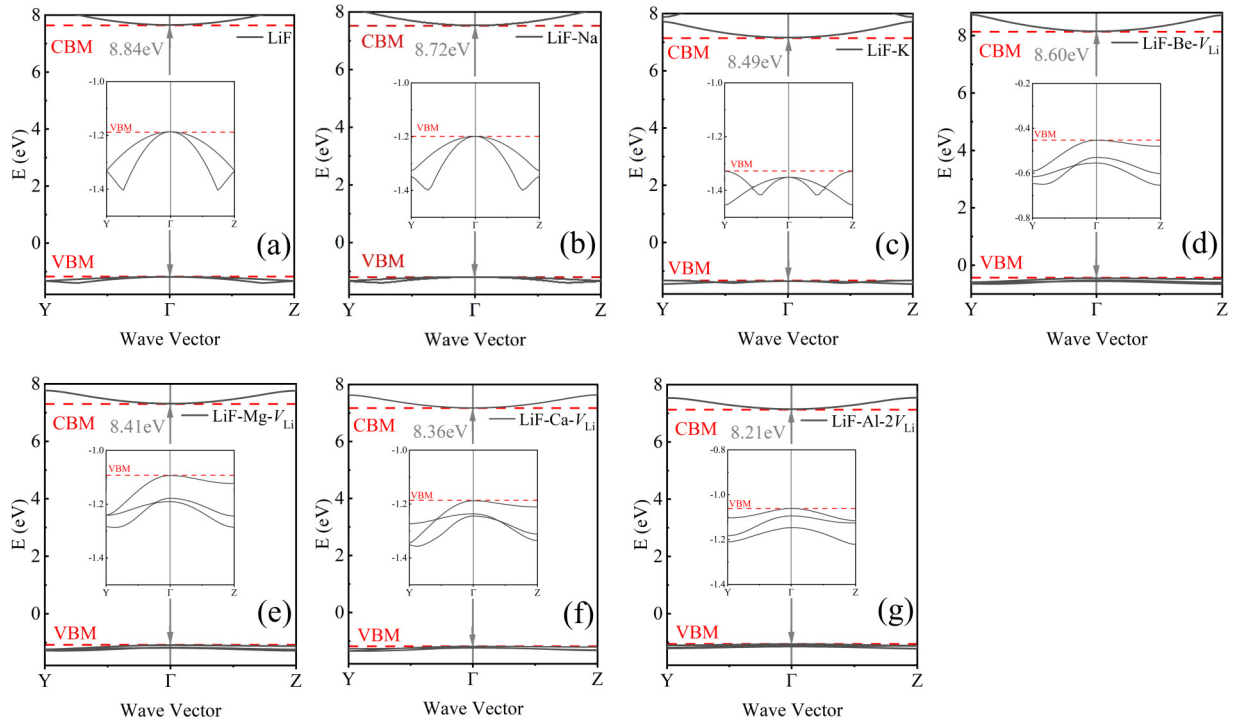
FIG. 4. The energy band structure of pure LiF and modified LiF.

magnitude increase in the Li-ion conductivity. Unlike the former, such a huge increase is mainly attributed to the concentration of $V_{\text{Li}}^-$. Clearly, the use of multivalent ion doping to introduce more $V_{\text{Li}}^-$ has greater potential to improve the Li-ion conductivity of LiF than regulating the Li-ion diffusion coefficient, but the influence of the doping effect on other properties still needs to be investigated.

It is worth mentioning that, as can be seen from Table I, multivalent ion doping greatly raises the defect concentration ($\sim$19 orders of magnitude) but decreases the Li-ion diffusion coefficient ($\sim$1 order of magnitude), which implies that there is still a possibility for LiF to further improve the Li-ion conductivity. In fact, Mukhopadhyay *et al.* [48] have achieved a simultaneous increase in defect concentration and lithium transport channel size in solid-state electrolytes using codoping techniques. Based on our calculations, the improvement of Li-ion diffusion coefficient by doping is much lower in order of magnitude than that of defect concentration, by only four orders of magnitude. Even so, further improvement of the Li-ion conductivity for modified LiF is still worth investigating in future work.

### 4. Electronic property

It is not expected to enhance the Li-ion conductivity of LiF while damaging other excellent properties. Here, we examine the influence of doping effects on electron conductivity of LiF. As shown in Fig. 4(a), pure LiF is a wide band gap crystal with three overlapping energy bands at the valence band maximum including one light hole and two heavy holes. Both the VBM and CBM are located at the $\Gamma$ point indicating that there is a direct band gap with the value is 8.84 eV. There is a small decrease in the band gap after doping, where the

band gap drops to 8.72, 8.49, 8.60, 8.41, 8.36, and 8.21 eV for $Na^+$, $K^+$, $Be^{2+}$, $Mg^{2+}$, $Ca^{2+}$, $Al^{3+}$, respectively. Even with the smallest band gap (8.21 eV), it is still a large value for the electron leap to the conduction band. Therefore, cation doping does not affect the band gap of LiF very much, and even this effect can be negligible. In comparison with Figs. 4(a)–4(c), it can be seen that the structure of the valence band maximum remains almost unchanged after $Na^+$ doping, while the energy of the VBM and CBM decreases and the band gap becomes indirect after $K^+$ doping. In Figs. 4(d)–4(g), similar structures with three heavy cavities are observed at the VBM after doping with multivalent ions.

To demonstrate that doping does not impair the electronic insulation of LiF, the electronic conductivity of LiF was further calculated. The electronic conductivity and all parameters related to it are listed in Table II. The electron effective masses $m_e^*$ of pure LiF is 0.52 $m_e$ and the electron concentration ($n_e$) counted by the Boltzmann distribution function Eq. (6) is $2.44 \times 10^{-32}$ cm$^{-3}$. The electron mobility ($\zeta_e$) in pure LiF obtained from the deformation potential theory is 111 cm$^2$/Vs. After doping, the changes in $m_e^*$, $n_e$ and $\zeta_e$ on the order of magnitude are very small. Furthermore, the electron conductivity ($\sigma_e$) in pure LiF and modified LiF is calculated by Eq. (13). As shown in Table II, the electronic conductivity of pure LiF is very low, only $4.33 \times 10^{-49}$ S/cm, while the order of magnitude of the $\sigma_e$ for the doped systems is still below $-45$, which indicates that the cation doping does not damage the electronic insulating property of LiF. We further calculated the band gaps using HSE06, which are generally 2.3 eV higher than before and closer to the experimental values (see Table S6 [20]). However, the electronic conductivity of LiF is extremely low by the GGA functional, and the result by the HSE06 functional will not change this conclusion.

TABLE II.  Parameters of electron conductivity for pure LiF and modified LiF.

| | Band gap (eV) | $m_e^*$ ($m_e$) | $n_e$ (cm$^{-3}$) | $\zeta_e$ (cm$^2$/Vs) | $\sigma_e$(S/cm) |
|---|---|---|---|---|---|
| LiF | 8.84 | 0.52 | $2.44 \times 10^{-32}$ | 111 | $4.33 \times 10^{-49}$ |
| LiF-Na | 8.72 | 0.51 | $4.76 \times 10^{-32}$ | 113 | $8.61 \times 10^{-49}$ |
| LiF-K | 8.49 | 0.47 | $9.74 \times 10^{-33}$ | 136 | $2.12 \times 10^{-49}$ |
| LiF-Be-$V_{\mathrm{Li}}$ | 8.60 | 0.51 | $1.97 \times 10^{-31}$ | 68 | $2.14 \times 10^{-48}$ |
| LiF-Mg-$V_{\mathrm{Li}}$ | 8.41 | 0.54 | $2.23 \times 10^{-31}$ | 158 | $5.64 \times 10^{-48}$ |
| LiF-Ca-$V_{\mathrm{Li}}$ | 8.36 | 0.52 | $3.35 \times 10^{-29}$ | 157 | $8.41 \times 10^{-46}$ |
| LiF-Al-$2V_{\mathrm{Li}}$ | 8.21 | 0.57 | $2.38 \times 10^{-29}$ | 105 | $4.00 \times 10^{-46}$ |

Previously, some research groups [49] have also regulated the defect/carrier concentration by precisely adjusting the chemical potential of the elements. In our study, both Li-ion conductivity and electron conductivity were very low under Li-rich condition. However, according to previous studies [13], when the elemental chemical potential is adjusted to Li-poor condition, the lithium vacancy and hole concentrations increase simultaneously, which is undesirable. Therefore, it is not possible to individually regulate performance by adjusting chemical potentials, and our work supports a good strategy to achieve a significant increase in Li-ion conductivity with little effect on electronic conductivity.

### 5. *Mechanical property*

We further discussed the mechanical properties of LiF including the bulk modulus ($B$), Young's modulus ($E$), shear modulus ($G$), and Poisson's ratio ($v$). For pure LiF, it has very good mechanical properties, with bulk modulus, Young's modulus, shear modulus, and Poisson's ratio are 70.34 GPa, 119.53 GPa, 49.12 GPa, and 0.217, respectively, which is sufficient to protect the SEI from puncturing by lithium dendrites. For doping Na$^+$, the mechanical properties are as excellent as those of pure LiF, but for doping with K$^+$, Be$^{2+}$, Mg$^{2+}$, Ca$^{2+}$, and Al$^{3+}$, there is a loss of mechanical properties to varying degrees, with the least loss for Mg$^{2+}$ doping. And the Poisson's ratio general increase except Be$^{2+}$ doping. In case of K$^+$ and Ca$^{2+}$ doping, the Poisson's ratio increase the most, which may owing to the volume expansion. However, if only the doping concentration we set are of concern, the mechanical property damage caused by doping is still within acceptable limits. It has been reported [50,51] that SEI films with Young's modulus greater than 6 GPa are sufficient to inhibit the growth of dendrites. Even with a minimum Young's modulus of 105 GPa for LiF-Al-$2V_{\mathrm{Li}}$, this is much greater than

TABLE III. Parameters of mechanical properties for pure LiF and modified LiF.

| | $B$ (GPa) | $E$ (GPa) | $G$ (GPa) | $v$ |
|---|---|---|---|---|
| LiF | 70.34 | 119.53 | 49.12 | 0.217 |
| LiF-Na | 71.18 | 119.75 | 49.09 | 0.220 |
| LiF-K | 67.80 | 106.64 | 43.07 | 0.238 |
| LiF-Be-$V_{\mathrm{Li}}$ | 61.93 | 106.78 | 44.03 | 0.213 |
| LiF-Mg-$V_{\mathrm{Li}}$ | 67.84 | 114.59 | 47.02 | 0.218 |
| LiF-Ca-$V_{\mathrm{Li}}$ | 66.30 | 106.18 | 43.06 | 0.233 |
| LiF-Al-$2V_{\mathrm{Li}}$ | 64.44 | 105.18 | 42.83 | 0.228 |

6 GPa. Therefore, we consider the effect of this doping concentration on the mechanical strength to be negligible. For the LiF bulk, doping with the multivalent ions Be$^{2+}$, Mg$^{2+}$, Ca$^{2+}$, and Al$^{3+}$ can substantially improve the Li-ion conductivity without compromising the electronic insulation and mechanical strength. Parameters of mechanical properties for pure LiF and modified LiF are shown in Table III. In the next sections, the LiF surface and the LiF-Li interface are further investigated in order to explore more fully the diffusion of Li across the SEI interface layer.

### B. LiF surface

The LiF(001) surface was built to simulate the Li-ion diffusion. Figures 5(a), 5(d) show two diffusion paths: (i) intralayer diffusion on the first atomic layer of the surface, path 1. (ii) diffusion from the first atomic layer to the second atomic layer, path 2. In Fig. 5(b), the diffusion energy barrier of Li ions for path1 (0.42 eV) is lower than the value for the bulk phase (0.56 eV), which indicates that the intralayer diffusion of Li ions on the surface is relatively easy. This is because there is less resistance to spatial sites and fewer bonds need to be broken for the diffusion process on the surface. Similar to LiF bulk, the diffusion energy barriers decrease to 0.38 eV and 0.40 eV after doping with Na$^+$ and K$^+$, while increase to 0.48, 0.43, 0.53, and 0.54 eV after doping with Be$^{2+}$, Mg$^{2+}$, Ca$^{2+}$, and Al$^{3+}$. The spatial effects and electrostatic interactions can also explain the above results. The average bond length at the saddle point is found to increase after the introduction of impurities, so $V_{\mathrm{Li}}^-$ in the Na$^+$ and K$^+$ doped system migrate more easily. In contrast, the $V_{\mathrm{Li}}^-$ in the Be$^{2+}$, Mg$^{2+}$, Ca$^{2+}$, and Al$^{3+}$ doped system are subjected to stronger electrostatic interactions and are therefore more difficult to migrate. The higher energy barrier of K$^+$ and Ca$^{2+}$, compared to the same main group elements, may be caused by the larger ionic radius and the smaller surface binding to the lattice, resulting in local lattice distortion (see Fig. S2 [20]). In Fig. 5(c), it is found that no charge transfer occurs during the migration of path1. In Fig. 5(e), the $V_{\mathrm{Li}}^-$ diffusion energy barrier of pure LiF for path 2 is 0.54 eV and the average bond length is 2.52 Å, which is close to bulk diffusion. The trends in the diffusion energy barriers and average bond lengths of vacancies remain in good agreement, indicating that spatial effects are still one of the factors dominating the migration of $V_{\mathrm{Li}}^-$. However, we note a different result from the previous discussion in that the diffusion barrier of the Be$^{2+}$, Mg$^{2+}$, Ca$^{2+}$, and Al$^{3+}$ doped system is lower than that of pure LiF, suggesting that the effect of electrostatic
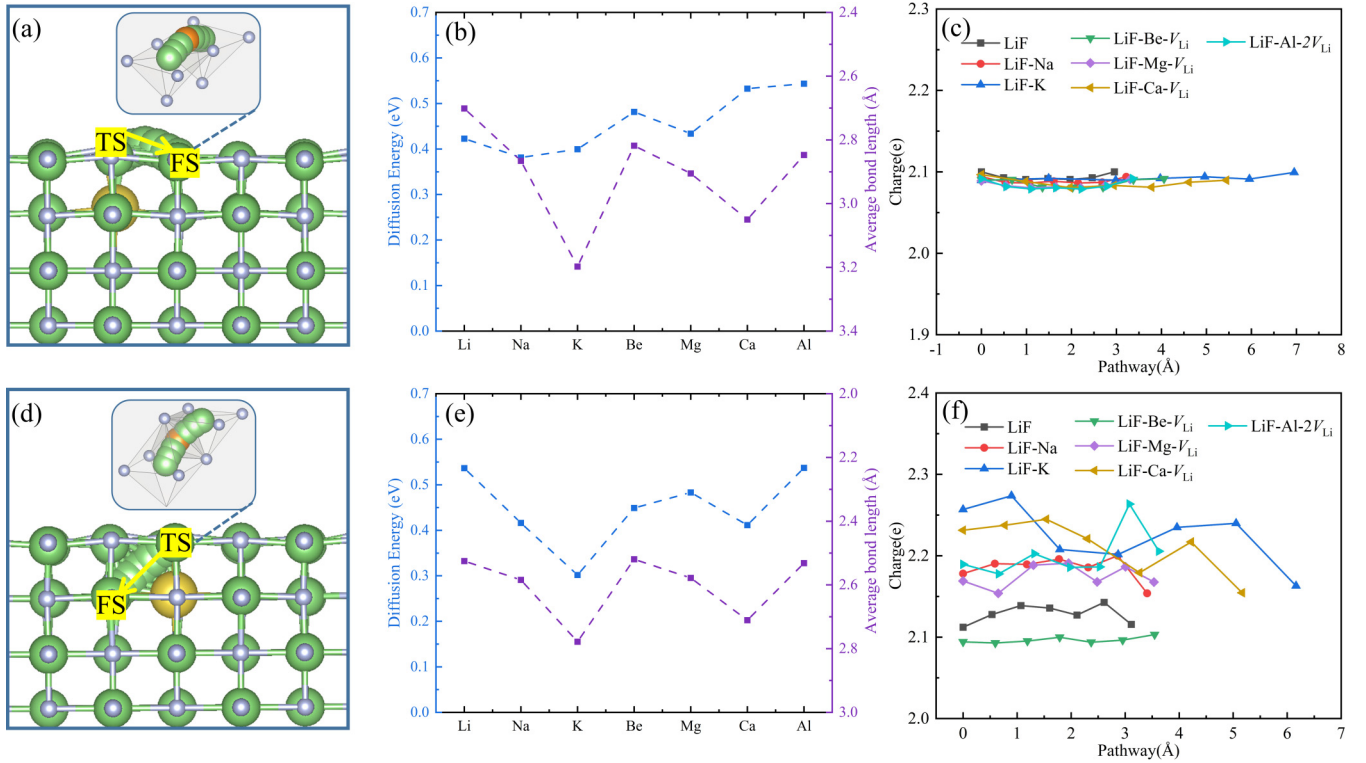
FIG. 5. (a), (d) Schematic diagram of the two $V_{Li}^-$ diffusion paths for the LiF(001) surface. TS is initial state and FS is final state. Yellow sphere represents $Na^+$, $K^+$, $Be^{2+}$, $Mg^{2+}$, $Ca^{2+}$, and $Al^{3+}$. Orange sphere represents the $Li^+$ at the saddle point. (b), (e) The diffusion energy barrier and the average bond lengths of migrating ions at the saddle point. (c), (f) The Bader charge value of $Li^+$ for each intermediate state during the diffusion of $V_{Li}^-$.

interactions on $V_{Li}^-$ migration is weakened. We think that this weakening may arise from the charge transfer during $V_{Li}^-$ migration. As shown in Fig. 5(f), charge transfer is present in path 2 for all systems, but is least pronounced in pure LiF and most pronounced in the $K^+$ and $Ca^{2+}$ doped system.

### C. LiF(001)-Li(001) interface

Figure 6(a) illustrates the LiF(001)-Li(001) interface model and the $V_{Li}^-$ diffusion path. Unlike before, since the Li metal layer has no F atoms, we calculate the average bond length between the migrating ions and the four nearest neighbors F ions at the saddle point. In Fig. 6(b), without doping, the diffusion barrier of $V_{Li}^-$ from the SEI into the Li layer is 0.44 eV and the average bond length is 2.44 Å, which suggests that the diffusion of Li ions at the interface is faster than in the bulk phase. It is clear that the diffusion energy barrier and the average bond length show a high degree of agreement. This implies that the electrostatic interaction between the dopant ion and the $V_{Li}^-$ is weakened. Figure 6(c) demonstrates that the valence states of the multivalent dopant ions at the LiF-Li interface are all reduced to varying degrees, which allows for easy migration of $V_{Li}^-$. On the other hand, significant charge transfer was also found for the migrating Li ions as shown in Fig. 6(d). This mainly originates from ionic bond breaking and metal bond creating, and may also weaken the binding of dopant ions to $V_{Li}^-$. We also found that during $V_{Li}^-$ migration, the charge transfer was single peaked for all systems except for the $K^+$ doped system, which was double peaked. This is

due to the fact that the larger lattice expansion (see Fig. S4 [20]) makes the diffusion channels longer and therefore a turning point appears [see Fig. 6(a)].

### IV. CONCLUSIONS

We have investigated the Li-ion conductivity of LiF after doping with $Na^+$, $K^+$, $Be^{2+}$, $Mg^{2+}$, $Ca^{2+}$, and $Al^{3+}$ using first-principles calculations. The defect formation energy results show that when doping with multivalent ions, $V_{Li}^-$ is generated to maintain the charge balance of the system. For diffusion kinetics, doping with $Na^+$ and $K^+$ are favorable for the $V_{Li}^-$ diffusion, while doping with $Be^{2+}$, $Mg^{2+}$, $Ca^{2+}$, and $Al^{3+}$ make the $V_{Li}^-$ diffusion more difficult. It was also found that the doping with both monovalent and multivalent ions improve the Li-ion conductivity, however, the mechanisms are different for the two. Doping with $Na^+$ and $K^+$ slightly improve Li-ion conductivity mainly by increasing the Li-ion diffusivity, whereas doping with multivalent ions substantially improved Li-ion conductivity by increasing defect concentration. Furthermore, our results show that the impairment of electronic conductivity and mechanical strength by low concentration doping is insignificant and negligible. We also considered Li-ion transport on the LiF(001) surface and at the LiF(001)-Li(001) interface to fully simulate the Li-ion diffusion across the SEI layer. Our results demonstrate that doping with $Na^+$, $K^+$, $Be^{2+}$, $Mg^{2+}$, $Ca^{2+}$, and $Al^{3+}$ ions improves the transport of Li ions in the bulk phase, on the surface and at the interface. This theoretical calculation provides good
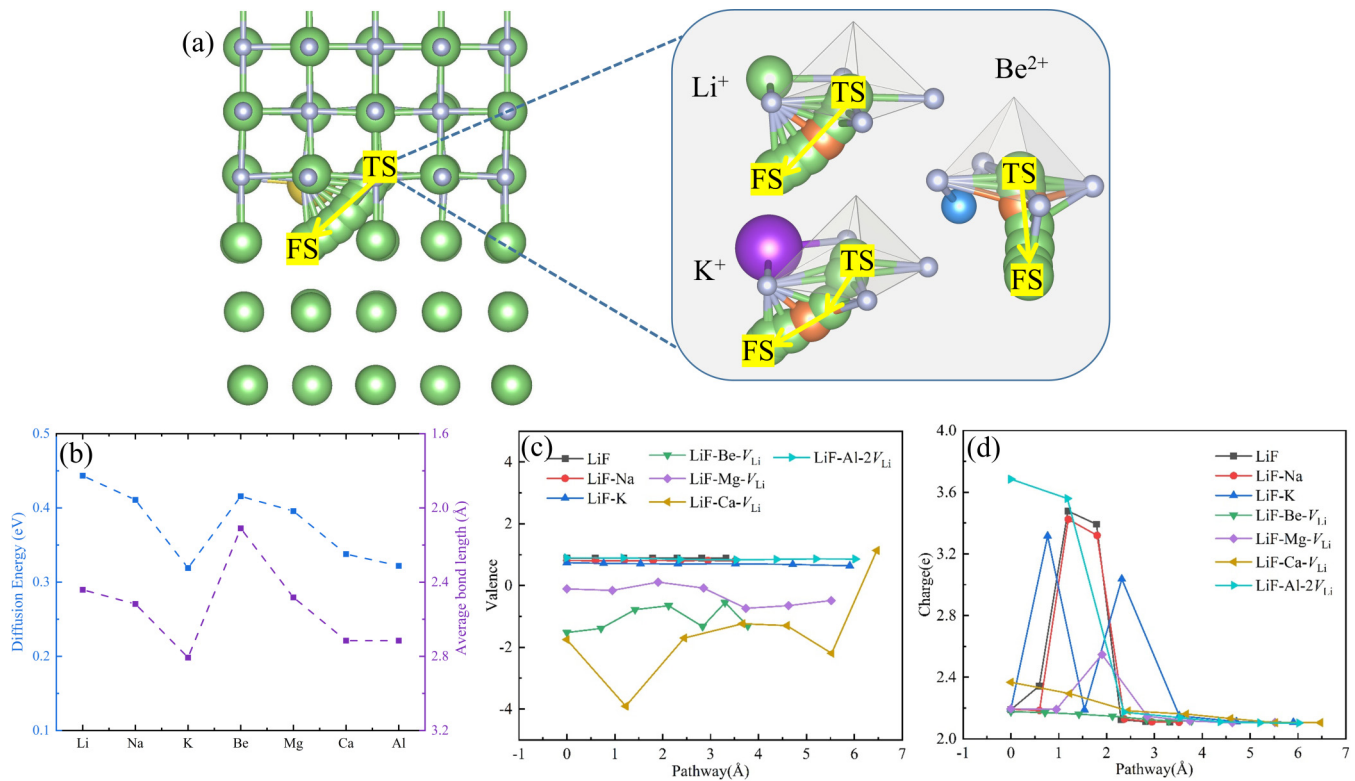
FIG. 6. (a) Schematic diagram of the $V_{Li}^-$ diffusion path for the LiF(001)-Li(001) interface. Yellow sphere represents $Na^+$, $K^+$, $Be^{2+}$, $Mg^{2+}$, $Ca^{2+}$, and $Al^{3+}$. Orange sphere represents the $Li^+$ at the saddle point. The partial highlighted view shows local diffusion paths of $V_{Li}^-$ for pure LiF, LiF-K, and LiF-Be, purple and blue spheres represent $K^+$ and $Be^{2+}$, respectively. (b) The diffusion energy barrier and the average bond lengths of migrating ions at the saddle point. (c) Valence change of doped atoms during the diffusion of $V_{Li}^-$. (d)The Bader charge transfer value of $Li^+$ for each intermediate state during the diffusion of $V_{Li}^-$.

inspiration for the experimental preparation of artificial SEI and good demonstration in independently tuning the ionic conductivity of materials. When trying to improve one property of a material, we should also consider whether other functional properties are affected.

Our strategy may also be applicable to other SEI materials. For example, $Li_3N$ has high Li-ion conductivity but also high electronic conductivity. Doping can be used to increase the band gap or reduce the carrier concentration. Additionally, in order to combine the advantages of different SEI components, we suggest applying composite structures with more SEI components mixed in. For example, a mixture of $Li_3N$ with high ionic conductivity and LiF with electronic insulation can be used.

[1] J. Tan, J. Matz, P. Dong, J. Shen, and M. Ye, A growing appreciation for the role of LiF in the solid electrolyte interphase, Adv. Energy Mater. **11**, 2100046 (2021).

[2] J. Zheng, Z. Ju, B. Zhang, J. Nai, T. Liu, Y. Liu, Q. Xie, W. Zhang, Y. Wang, and X. Tao, Lithium ion diffusion mechanism on the inorganic components of the solid-electrolyte interphase, J. Mater. Chem. A **9**, 10251 (2021).

[3] X. Fan, L. Chen, O. Borodin, X. Ji, J. Chen, S. Hou, T. Deng, J. Zheng, C. Yang, S.-C. Liou, K. Amine, K. Xu, and C. Wang, Non-flammable electrolyte enables Li-metal batteries with aggressive cathode chemistries, Nature Nanotechnol. **13**, 1191 (2018).

[4] X.-Q. Zhang, X. Chen, X.-B. Cheng, B.-Q. Li, X. Shen, C. Yan, J.-Q. Huang, and Q. Zhang, Highly stable lithium metal batteries enabled by regulating the solvation of lithium ions in nonaqueous electrolytes, Angew. Chem. Int. Ed. **57**, 5301 (2018).

[5] J. Xie, L. Liao, Y. Gong, Y. Li, F. Shi, A. Pei, J. Sun, R. Zhang, B. Kong, R. Subbaraman, J. Christensen, and Y. Cui, Stitching h-BN by atomic layer deposition of LiF as a stable interface for lithium metal anode, Sci. Adv. **3**, eaao3170 (2017).

[6] J. Lang, Y. Long, J. Qu, X. Luo, H. Wei, K. Huang, H. Zhang, L. Qi, Q. Zhang, Z. Li, and H. Wu, One-pot solution coating of high quality LiF layer to stabilize Li metal anode, Energy Stor. Mater. **16**, 85 (2019).

[7] G. Geschwind, Low-temperature electrical conductivity in calcium-doped lithium fluoride, J. Am. Ceram. Soc. **51**, 539 (1968).

[8] S. Lorger, K. Narita, R. Usiskin, and J. Maier, Enhanced ion transport in $Li_2O$ and $Li_2S$ films, Chem. Commun. **57**, 6503 (2021).

[9] Y. X. Ren, L. Zeng, H. R. Jiang, W. Q. Ruan, Q. Chen, and T. S. Zhao, Rational design of spontaneous reactions for protecting porous lithium electrodes in lithium-sulfur batteries, Nature Commun. **10**, 3249 (2019).

[10] G. G. Eshetu, X. Judez, C. Li, O. Bondarchuk, L. M. Rodriguez-Martinez, H. Zhang, and M. Armand, Lithium azide as an electrolyte additive for all-solid-state lithium-sulfur batteries, Angew. Chem. Int. Ed. **56**, 15368 (2017).

[11] A. Hu, W. Chen, X. Du, Y. Hu, T. Lei, H. Wang, L. Xue, Y. Li, H. Sun, Y. Yan, J. Long, C. Shu, J. Zhu, B. Li, X. Wang, and J. Xiong, An artificial hybrid interphase for an ultrahigh-rate and practical lithium metal anode, Energy Environ. Sci. **14**, 4115 (2021).

[12] Y. Ren, Z. Qi, X. Ma, S. Yang, C. Zhang, X. Tan, and X. Liu, First-principles study of the effect of mechanical strength on ion transport in La-doped LiF-SEI on the Li (001) surface, Mater. Today Chem. **20**, 100451 (2021).

[13] J. Pan, Y.-T. Cheng, and Y. Qi, General method to predict voltage-dependent ionic conduction in a solid electrolyte coating on electrodes, Phys. Rev. B **91**, 134116 (2015).

[14] G. Kresse and J. Furthmuller, Efficient iterative schemes for ab initio total-energy calculations using a plane-wave basis set, Phys. Rev. B **54**, 11169 (1996).

[15] J. P. Perdew, J. A. Chevary, S. H. Vosko, K. A. Jackson, M. R. Pederson, D. J. Singh, and C. Fiolhais, Atoms, molecules, solids, and surfaces - applications of the generalized gradient appoximation for exchange and correlation, Phys. Rev. B **46**, 6671 (1992).

[16] D. R. Hamann, Optimized norm-conserving vanderbilt pseudopotentials, Phys. Rev. B **88**, 085117 (2013).

[17] N. Ashcroft and N. Mermin, *Solid State Physics, Science: Physics* (Saunders College, Philadelphia, 1976).

[18] D. B. Sirdeshmukh, L. Sirdeshmukh, and K. G. Subhadra, *Alkali Halides: A Handbook of Physical Properties, Materials Science Series* (Springer, Berlin, 2001).

[19] A. Ramasubramanian, V. Yurkiv, T. Foroozan, M. Ragone, R. Shahbazian-Yassar, and F. l. Mashayek, Lithium diffusion mechanism through solid-electrolyte interphase in rechargeable lithium batteries, J. Phys. Chem. C **123**, 10237 (2019).

[20] See Supplemental Material at http://link.aps.org/supplemental/10.1103/PhysRevMaterials.8.015403 for the models of bulk LiF; the (001) surface of LiF and LiF(001) − Li(001) interface; the screening process of dopant atoms; the defect formation energy of LiF-Be, LiF-Mg, and LiF-Ca; the local volume expansion after doping; the parameters for calculating the defect concentration; the band gaps calculated by GGA and HSE06; and the arrangements of dopants and vacancies.

[21] G. Henkelman, B. Uberuaga, and H. Jonsson, A climbing image nudged elastic band method for finding saddle points and minimum energy paths, J. Chem. Phys. **113**, 9901 (2000).

[22] N. A. Zarkevich and D. D. Johnson, Nudged-elastic band method with two climbing images: Finding transition states in complex energy landscapes, J. Chem. Phys. **142**, 024106 (2015).

[23] J. Heyd, G. E. Scuseria, and M. Ernzerhof, Hybrid functionals based on a screened coulomb potential, J. Chem. Phys. **118**, 8207 (2003).

[24] W. Jia, Z. Cao, L. Wang, J. Fu, X. Chi, W. Gao, and L.-W. Wang, The analysis of a plane wave pseudopotential density functional theory code on a GPU machine, Comput. Phys. Commun. **184**, 9 (2013).

[25] W. Tang, E. Sanville, and G. Henkelman, A grid-based bader analysis algorithm without lattice bias, J. Phys.: Condens. Matter **21**, 084204 (2009).

[26] M. Yu and D. R. Trinkle, Accurate and efficient algorithm for Bader charge integration, J. Chem. Phys. **134**, 064111 (2011).

[27] S. B. Zhang and J. E. Northrup, Chemical potential dependence of defect formation energies in GaAs: Application to Ga self-diffusion, Phys. Rev. Lett. **67**, 2339 (1991).

[28] C. G. Van de Walle and P. E. Blöchl, First-principles calculations of hyperfine parameters, Phys. Rev. B **47**, 4244 (1993).

[29] C. Van de Walle and J. Neugebauer, First-principles calculations for defects and impurities: Applications to III-Nitrides, J. Appl. Phys. **95**, 3851 (2004).

[30] J. Goodenough and Y. Kim, Challenges for rechargeable batteries, J. Power Sources **196**, 6688 (2011).

[31] H.-P. Komsa, T. T. Rantala, and A. Pasquarello, Finite-size supercell correction schemes for charged defect calculations, Phys. Rev. B **86**, 045112 (2012).

[32] S. Lany and A. Zunger, Assessment of correction methods for the band-gap problem and for finite-size effects in supercell defect calculations: Case studies for ZnO and GaAs, Phys. Rev. B **78**, 235104 (2008).

[33] S. Shi Jr., P. Lu, Z. Liu, Y. Qi, L. Hector, H. Li, and S. Harris, Direct calculation of Li-ion transport in the solid electrolyte interphase, J. Am. Chem. Soc. **134**, 15476 (2012).

[34] S. Shi Jr., Y. Qi, H. Li, and J. G., Defect thermodynamics and diffusion mechanisms in $Li_2CO_3$ and implications for the solid electrolyte interphase in Li-ion batteries, J. Phys. Chem. C **117**, 8579 (2013).

[35] D. B. Laks, C. G. Van de Walle, G. F. Neumark, and S. T. Pantelides, Role of native defects in wide-band-gap semiconductors, Phys. Rev. Lett. **66**, 648 (1991).

[36] J.-H. Yang, W.-J. Yin, J.-S. Park, and S.-H. Wei, Self-regulation of charged defect compensation and formation energy pinning in semiconductors, Sci. Rep. **5**, 16977 (2015).

[37] A. Van der Ven, G. Ceder, M. Asta, and P. D. Tepesch, First-principles theory of ionic diffusion with nondilute carriers, Phys. Rev. B **64**, 184307 (2001).

[38] J. Lee, Z. Deng, N. C. Bristowe, P. D. Bristowe, and A. K. Cheetham, The competition between mechanical stability and charge carrier mobility in MA-based hybrid perovskites: Insight from DFT, J. Mater. Chem. C **6**, 12252 (2018).

[39] T. Zhao, W. Shi, J. Xi, D. Wang, and Z. Shuai, Intrinsic and extrinsic charge transport in $CH_3NH_3PbI_3$ perovskites predicted from first-principles, Sci. Rep. **6**, 19968 (2016).

[40] N. Birks and G. H. Meier, *Introduction to High Temperature Oxidation of Metals* (Edward Arnold Publishers, London, 1983).

[41] D. Gerasimov, The Nernst–Einstein equation for an anomalous diffusion at short spatial scales, Physica D **419**, 132851 (2021).

[42] Y. Li, P. Canepa, and P. Gorai, Role of electronic passivation in stabilizing the Lithium-$Li_xPO_yN_z$ solid-electrolyte interphase, PRX Energy **1**, 023004 (2022).

[43] C. Kittel and D. F. Holcomb, Introduction to solid state physics, Am. J. Phys. **35**, 547 (1967).

[44] J. Liu, M. Weng, S. Li, X. Chen, J. Cen, J. Jie, W. Xiao, J. Zheng, and F. Pan, High-throughput HSE study on the doping effect in anatase TiO$_2$, Phys. Chem. Chem. Phys. **22**, 39 (2020).

[45] L. Guo, X. Zheng, and Z. Zeng, Transition metal encapsulated hydrogenated silicon nanotubes: Silicon-Based Half-Metal, Phys. Lett. A **375**, 4209 (2011).

[46] H. Yildirim, A. Kinaci, M. K. Y. Chan, and J. P. Greeley, First-principles analysis of defect thermodynamics and ion transport in inorganic SEI compounds: LiF and NaF, ACS Appl. Mater. Interfaces **7**, 18985 (2015).

[47] M. Adam-Benveniste, *Study of the Electrical Conductivity of Lithium Fluoride*, Report (Comm. Energie Atomique, Saclay, France, 1969).

[48] S. Mukhopadhyay, T. Thompson, J. Sakamoto, A. Huq, J. Wolfenstine, J. Allen, N. Bernstein, D. Stewart, and M. Johannes, Structure and stoichiometry in supervalent doped Li$_7$La$_3$Zr$_2$O$_{12}$, Chem. Mater. **27**, 3658 (2015).

[49] P. Gorai, T. Famprikis, B. Singh, V. Stevanovic, and P. Canepa, Devil is in the defects: Electronic conductivity in solid electrolytes, Chem. Mater. **33**, 7484 (2021).

[50] C. Monroe and J. Newman, Dendrite growth in lithium/polymer systems – a propagation model for liquid electrolytes under galvanostatic conditions, J. Electrochem. Soc. **150**, A1377 (2003).

[51] G. M. Stone, S. A. Mullin, A. A. Teran, D. T. Hallinan, A. M. Minor, A. Hexemer, and N. P. Balsara, Resolution of the modulus versus adhesion dilemma in solid polymer electrolytes for rechargeable lithium metal batteries, J. Electrochem. Soc. **159**, A222 (2011).